Complex demodulation applied to Pi2 geomagnetic pulsations

D. Beamish *Institute of Geological Sciences, Murchison House, West Mains Road, Edinburgh EH9 3LA*

H. W. Hanson and D. C. Webb *Department of Physics, University of York, Heslington, York Y01 5DD*

Beamish, D., Hanson, H.W. and Webb, D.C., 1979. Complex demodulation applied to Pi2 geomagnetic pulsations. Geophys. J. R. astr. Soc., 58, 471-493
DOI: 10.1111/j.1365-246X.1979.tb01035.x

Summary. The spectral technique of complex demodulation is applied to Pi2 pulsations recorded along a meridional profile. The technique provides instantaneous values of amplitude and phase and allows frequency dispersion to be taken into account. The variations of magnetospheric wave polarization parameters are observed as a function of both space and time. The results are directly compared with recent theories of the resonance of geomagnetic field lines and the effects of the ionosphere on ground based observations. The theoretical predictions are tested and the experimental results indicate that the night-time ionosphere is capable of a controlling influence on the source characteristics of these magnetospheric waves in the plasmapause region.

Introduction

In many geophysical applications the frequency spectrum of a time varying parameter is obtained from the Fourier coefficients derived from the Fast Fourier Transform (FFT). As a first stage in the analysis of a geomagnetic time series consisting of a mixture of noise and harmonic oscillations, the raw unsmoothed Fourier coefficients give a representation of the frequency content of the time series.

Fig. 1(a)–(d) show raw amplitude spectra of the horizontal field intensity recorded at different sampling rates at Eskdalemuir. Each data series consists of 480 data points and has been prepared for the FFT in the usual way by reducing the raw data series to zero mean and zero linear trend; the ends being tapered to zero and further zeros added to bring the now modified data series up to 512 points.

Fig. 1(a) shows the raw amplitude spectrum of 480 monthly means spanning 40 yr. At the longest periods a continuum of activity is evident with the 11-yr solar-cycle dominant. At shorter periods the 12 and 6 month harmonics are well defined against a background of white noise. Fig. 1(b) is the spectrum obtained from 480 hourly means (20 days in total). A white noise process is again exhibited with well-defined harmonic peaks with periods of 24 and 12 hr. The raw amplitude spectrum obtained from 480 min values (8 hr) is shown in

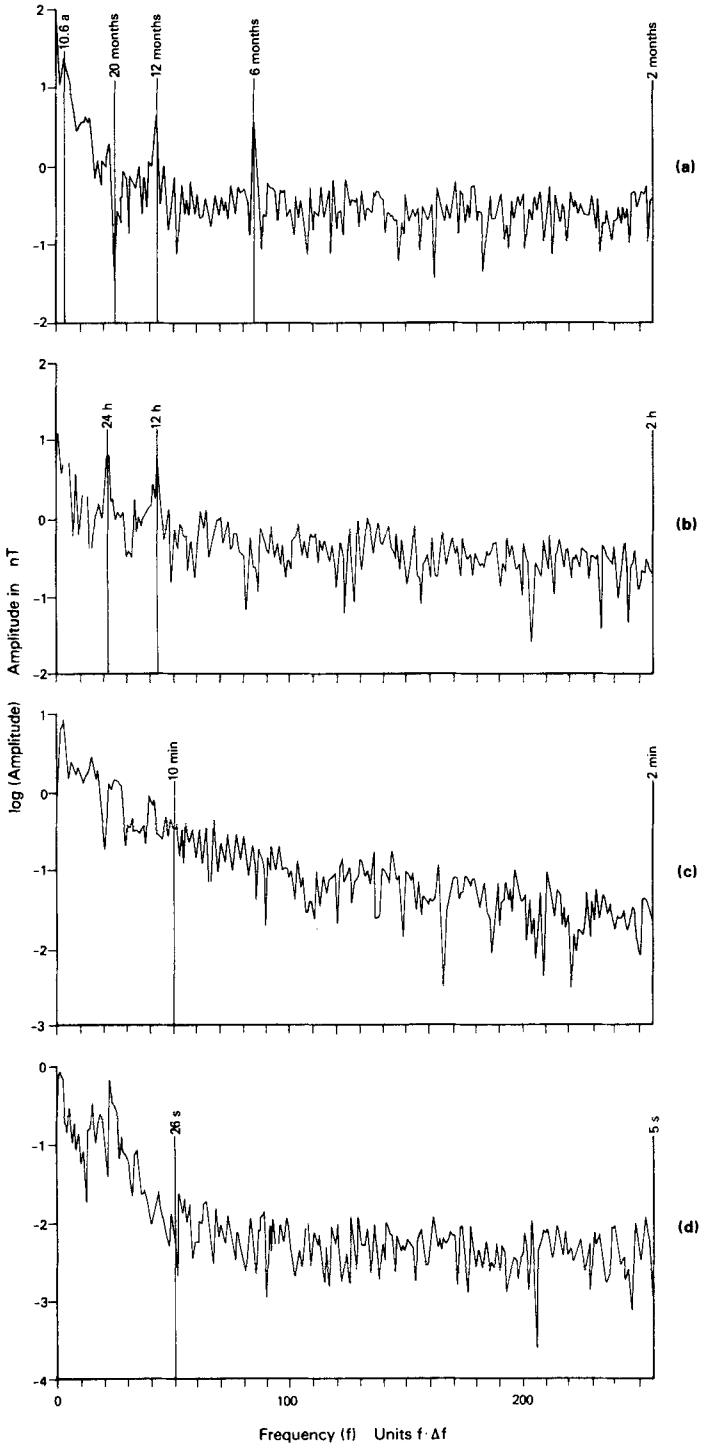

Figure 1. Raw amplitude spectra of the horizontal field intensity at Eskdalemuir. (a) Monthly means 1930–70, $\Delta f = 1/512$ cycle/month. (b) Hourly means 1958 January 1–1958 January 20, $\Delta f = 1/512$ cycle/hr. (c) Minute means, $\Delta f = 1/512$ cycle/min. (d) 2.5 s values, $\Delta f = 1/1280$ cycle/s.

Fig. 1(c). This data sample contains substorm activity and the spectrum indicates no harmonic structure; instead there is a continuum of periodicities extending to the Nyquist period. Fig. 1(d) shows the raw amplitude spectrum obtained from 480 2.5 s values (20 min). This data sample was recorded during typical daytime continuous pulsation activity. At periods greater than 26 s a non-harmonic continuum of periodicities exists while at periods less than 26 s a white noise process is evident.

From the above considerations it is clear that the statistical stability of geomagnetic spectra at periods less than 12 hr is of major importance. In order to improve the reliability of the spectral estimates a second stage in the analysis is often undertaken. The frequency resolution of the raw FFT can be sacrificed and spectral smoothing employed (see Stuart, Sherwood & Mackintosh 1971). For example, the effect of smoothing the raw amplitude spectrum of Fig. 1(d) is shown in Fig. 2. The smoothing employed is analagous to that described by Stuart *et al.* (1971) with 128 lags being used. In addition, a zero phase shift, high-pass filter has been used such that the spectrum below 150 s is unaffected. The relatively broad-band nature of the continuous pulsation activity with a central peak at 53 s is observed more clearly in Fig. 2.

Geomagnetic pulsation events exhibit a wide variety of spectral forms; see for examples the review by Orr (1973). Fig. 1(a) (Orr 1973) shows a succession of lightly damped continuous pulsation bursts which are phase shifted with respect to each other. Figs 1(b) and 2 (Orr 1973) give examples of pulsations which show frequency dispersion while Fig. 7 is typical of a heavily damped night-time pulsation. A third stage in the analysis procedure of geomagnetic pulsations is required to take into account the fact that, in general, the signals are non-stationary and can exhibit frequency dispersion. The application of complex demodulation techniques, described in the following sections, facilitates the examination of such behaviour.

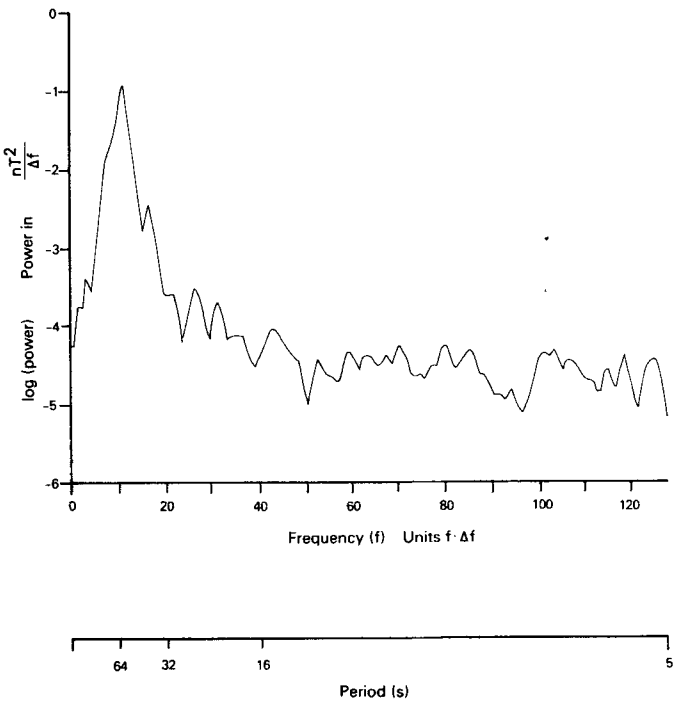

Figure 2. Smoothed power spectrum of 2.5 s value data file used in Fig. 1(d), $f = 1/640$ cycle/s.

Definition and computation of complex demodulates

The technique of complex demodulation of a time-series is described fully in a paper by Bingham, Godfrey & Tukey (1967). Previously Tukey (1961) had said of complex demodulation, 'It has to be tried out on actual data before its incisiveness and power is adequately appreciated'. More recently, however, Banks (1975) has drawn attention to the usefulness of the technique when applied to geomagnetic time-series. Drawing on the above two papers, we have assessed its applicability to pulsation analysis. The technique allows the amplitude and phase of spectral components of a time-series to be re-expressed in the time-domain. The mathematical description of the procedure involves two stages. Firstly, a frequency band of interest (centred on frequency ω' say) is shifted to zero frequency by multiplying each term of the time-series $x(t)$ by the complex function $\exp(-i\omega' t)$:

$$X_s(\omega', t) = x(t) \exp(-i\omega' t). \tag{1}$$

Secondly, the new frequency-shifted series $X_s(\omega', t)$ is then low-pass filtered using a set of weights (a_k) to produce the demodulated time-series $X_d(\omega', t)$, i.e.

$$X_d(\omega', t) = \sum_{k=-m}^{k=m} a_k X_s(\omega', t + k\Delta t). \tag{2}$$

Alternatively, this demodulated time-series may be expressed in terms of its modulus and phase as:

$$X_d(\omega', t) = |X_d(\omega', t)| \exp[-i\phi(\omega', t)]. \tag{3}$$

The most efficient way of obtaining the complex demodulates is based on the FFT and is described by Banks (1975). The raw data series is prepared for the FFT in the normal way and the Fourier Transform computed. The resulting real and imaginary Fourier coefficients are then multiplied by a chosen set of weights (a band-pass filter centred on ω'); the resulting band of frequencies being shifted to zero frequency. The new set of low-frequency Fourier coefficients are then truncated (equivalent to defining a new Nyquist frequency ω'_N) so as to produce a demodulated frequency-series consisting of independent data points. Finally, an inverse FFT converts the coefficients back into the time domain thereby generating the time-series of complex demodulates centred on ω' and with new sampling interval $\Delta t' = (1/2\omega'_N)$.

The only real computational problem arising in the above procedure is in the choice of a band-pass filter. A knowledge of the frequency band of interest in relation to the other possible frequency components of the time-series is required. This information is obtained from the spectrum of the time-series. The application of complex demodulation to harmonic signals, such as the daily variation, is described by Banks (1975). In such cases, the design of a discrete function of frequency centred on the periodic component of interest is straightforward since the neighbouring frequency components consist of white noise. For non-harmonic signals, such as may be encountered in pulsation analysis, however, care must be taken with regard to filter design.

An appropriate set of weights to use in the frequency domain is a band-pass Hanning window $W(\omega)$:

$$W(\omega) = 0.5\left[1 + \cos 2\frac{\pi(\omega - \omega')}{\Delta\omega}\right] \qquad \omega' - \frac{\Delta\omega}{2} \leqslant \omega \leqslant \omega' + \frac{\Delta\omega}{2} \tag{4}$$

$$= 0 \text{ elsewhere.}$$

Here ω' is again the central frequency of the band of width $\Delta\omega$. To allow a good definition of wider-band signals such as pulsations, a box-car modified by half-cosine bells can be used (Banks 1975).

The multiplication of the raw Fourier coefficients by such a filter constitutes a smoothing of the raw demodulates $X_s(\omega', t)$. From equation (4) it can be seen that for small $\Delta\omega$, $W(\omega)$ approaches unity, i.e. it becomes constant and independent of ω. This is equivalent to imposing a low resolution but obtaining a high stability for the demodulates. In this case, if $\Delta\omega$ is much less than the true width of a spectral peak, as may be the case for broad-band signals, then the resulting demodulates will be undersampled and will tend to reflect filter rather than signal behaviour. Conversely, a large $\Delta\omega$ leads to high resolution and low stability. In this case if $\Delta\omega$ is much greater than the true width of a spectral peak then the resulting demodulates will be oversampled and the demodulates will not be independent and therefore may not necessarily reflect true signal behaviour. The band-pass filter should be designed such that $\Delta\omega$ is approximately the same width as the spectral peak of interest; $\Delta\omega$ will then determine both the number of *independent* points required to specify fully the demodulated series in the time domain and the number of frequency components used in forming the demodulated series.

If the time-series under consideration defines a stationary Gaussian process then its spectrum would have the sampling distribution of a chi-square process. Under such circumstances confidence limits could be placed on the demodulated series using the number of degrees of freedom of the analysis. Cooley, Lewis & Welch (1967) give the equivalent degrees of freedom (μ) of such a distribution as:

$$\mu = \frac{N\pi}{\Delta\omega^*} \tag{5}$$

where N is the number of raw unmodified data points and $\Delta\omega^*$ is the 'half-power' width of the filter. The natural bandwidth of a typical pulsation (Fig. 2) suggests that the process is non-stationary. However, as Bingham *et al.* (1967) point out, the behaviour of individual values of the demodulates depends on relatively time-local or instantaneous properties of the series. Accordingly, the time-local properties of the complex demodulates can be used to estimate the character of this non-stationority.

Referring to Bingham *et al.* (1967) and equations (1) and (2), the first stage in the complex demodulation of a *periodic* time-series:

$$x(t) = \cos(\omega_0 t + \gamma)$$

produces the frequency-shifted demodulates:

$$X_s(\omega', t) = \frac{A}{2}\exp\left[-i(\delta\omega \cdot t - \gamma)\right] + \exp\left\{-i\left[(2\omega_0 + \delta\omega)t + \gamma\right]\right\}$$

where $X_s(\omega', t)$ is centred on the frequency $\omega' = \omega_0 + \delta\omega$ and therefore contains components at the frequencies $-\delta\omega$ and $-(2\omega_0 + \delta\omega)$. The second stage of the procedure is to low-pass $X_s(\omega', t)$ and remove the component at $-(2\omega_0 + \delta\omega)$ leaving:

$$X_d(\omega_0 + \delta\omega, t) = \frac{A}{2}\exp\left[-i(\delta\omega \cdot t - \gamma)\right]. \tag{6}$$

The phase ϕ_d of the demodulate is therefore:

$$\phi_d = -\delta\omega \cdot t + \gamma \tag{7}$$

and the phase of a computationally derived demodulated series will thus exhibit a linear

gradient of $-\delta\omega$ which will reverse sign about the central frequency ω_0. If, however, the central frequency of the band-pass filter is chosen such that $\omega' = \omega_0$ then $\delta\omega = 0$ and equation (6) reduces to:

$$X_d(\omega_0, t) = \frac{A}{2} \exp(i\gamma). \tag{8}$$

In this case if the amplitude (A) and phase (γ) of the original time-series change with time then the nature of this change will be demonstrated in the demodulated series. The procedure of complex demodulation therefore allows two important aspects of pulsation behaviour to be examined and quantified. In the first instance, the precise determination of the central frequency of the band of frequencies defining a pulsation event and, secondly, demodulation at this central frequency then allows the determination of the temporal characteristics of both amplitude and phase throughout the pulsation event.

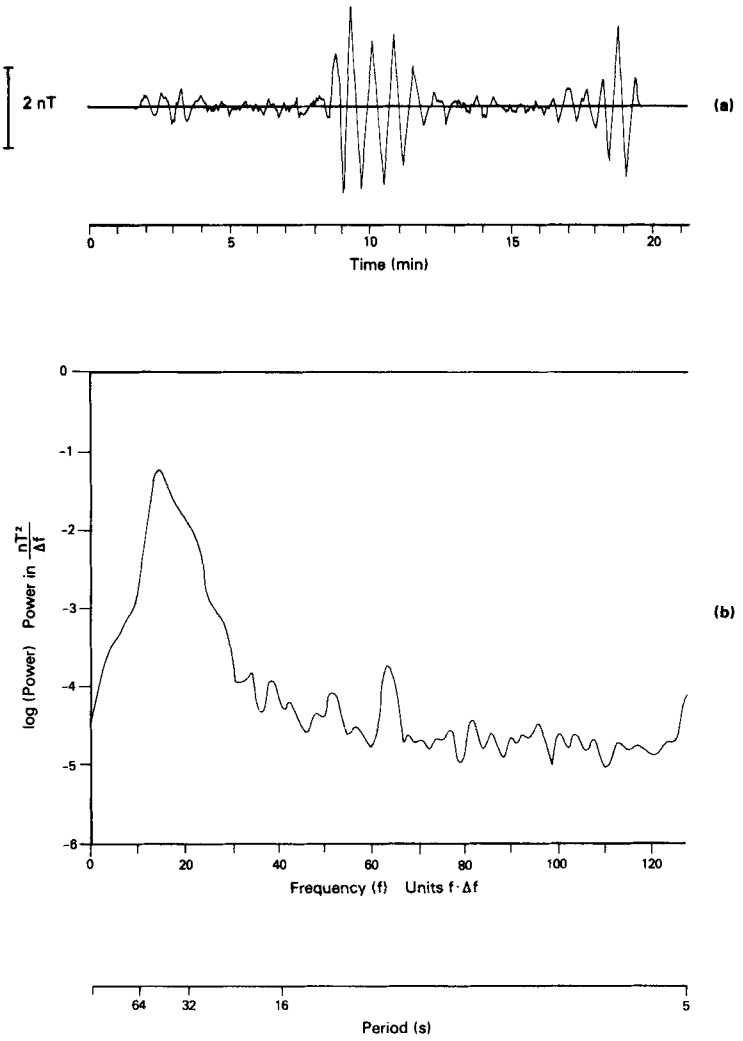

Figure 3. (a) Impulsive night-time Pi2 in the H-component at Lerwick. Time 0 corresponds to 01.67 UT on 1976 March 14. (b) Smoothed power spectrum of waveform of (a), $\Delta f = 1/640$ cycle/s.

Application to a dispersive Pi2 waveform

(a) DETERMINATION OF COMPLEX DEMODULATES

To demonstrate the application of complex demodulation to micropulsations we consider the waveform shown in Fig. 3(a). The waveform is an impulsive night-time Pi2 recorded in the H-component at Lerwick, one of an array of magnetometer stations operated by the Institute of Geological Sciences (see Table 1). This waveform is particularly appealing as both frequency dispersion and amplitude modulation are observed. The original data series consists of 20 min of data sampled at 2.5 s intervals. Fig. 3(a) shows the modified and high-pass filtered waveform. We confine our attention to the central portion which consists of five well-defined cycles of oscillation.

Table 1. Station coordinates used in the study.

Station	Mnemonic	Geomagnetic Co-ordinates* Latitude	Longitude	L-value**
Lerwick	Le	60.0	-135.4	3.8
Loch Laggan	Ll	57.6	-140.3	3.3
Earlyburn	Eb	56.2	-139.8	3.0
Eskdalemuir	Es	55.8	-140.0	3.0
York	Yo	54.2	-138.6	2.7
Hartland	Ha	52.0	-143.0	2.4

* Eccentric geomagnetic.
** IGRF 1975, 150 km altitude.

The smoothed power spectrum obtained using 128 lags is shown in Fig. 3(b). Within its limited resolution the spectral peak is found at a period of 42.5 s, with a half-log power width defined between periods of 98 and 22 s. To demonstrate the determination of the central frequency and to verify the arguments expressed in the previous section, a band-pass filter was designed as shown schematically in Fig. 4. Fig. 4(a) is an idealized representation of a power spectrum, the frequency axis being made up of the 'elementary' frequencies obtained from a direct FFT. The symmetrical band-pass filter shown in Fig. 4(b) has a weight of unity only at the central frequency ω_0 and tapers away to zero at the half-power points of the power spectrum (ω_1 and ω_2). Obviously such a filter will distort the content of the true power spectrum but will still pass the central frequency, ω_0, adequately. Such a filter has been used to examine the behaviour of the phase of the demodulates of the Pi2 waveform centred on differing ω_0. The chosen central frequencies correspond to periods of 47.4, 45.7, 44.1, 42.6 and 41.3 s and the phases of the resulting demodulates are shown in Fig. 5. The central frequencies chosen are successive 'elementary' frequencies of the raw FFT.

The time interval over which the phase estimates have been determined corresponds to the duration of the modified data series shown again for reference in Fig. 5. However the phase estimates have a sampling interval of 26.7 s. The time-local properties of the phase of a data series will only be accurately determined when the amplitude of the series rises above the noise level. We therefore restrict our attention to the behaviour of the phase within the solid vertical lines of Fig. 5. For the chosen central periods of 47.4 and 45.7 s, a predominant positive gradient of the phase is observed corresponding to a chosen ω_0 less than the correct central frequency (equation (7)). Conversely, for the chosen central periods of 42.6 and 41.3 s a predominant negative gradient is observed corresponding to a chosen

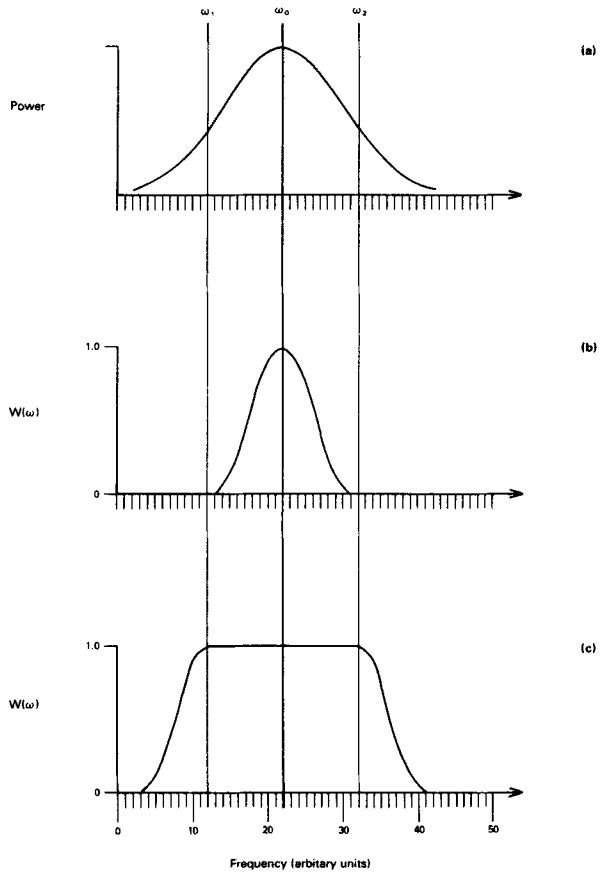

Figure 4. (a) Idealized power spectrum. (b) and (c) idealized frequency domain band-pass filters used in the analysis.

ω_0 greater than the correct central frequency. The condition represented by equation (8) is most clearly defined, for this data series, at a central frequency corresponding to a period of 44.1 s.

The filter used in the above procedure is essentially a computational recipe for the precise determination of the central frequency of a process. The filter used represents a condition of $\Delta\omega$ being much less than the width of the spectral peak. What is clear from Fig. 5 is that such an inadequate filter design will distort the phase estimates of the noise on each side of the signal (they are non-random) while the phase value obtained for the signal becomes a function of the central frequency of the filter.

Having established the correct central frequency for this waveform we now wish to design a band-pass filter to pass undistorted the spectral content shown in Fig. 3(b). The schematic filter adopted is shown in Fig. 4(c). To allow full definition of the spectral peak a box-car modified by half-cosine bells is required. To prevent phase distortion, the half-cosine bells should not operate within the half-power points of the spectral peak. Due to the wide-band nature of pulsation signals, the filter will necessarily extend into quite low frequencies (i.e. periods greater than 100 s), it is therefore necessary to high-pass filter the data in accordance with possible longer period processes. The high-pass filter applied to the present data is considered adequate.

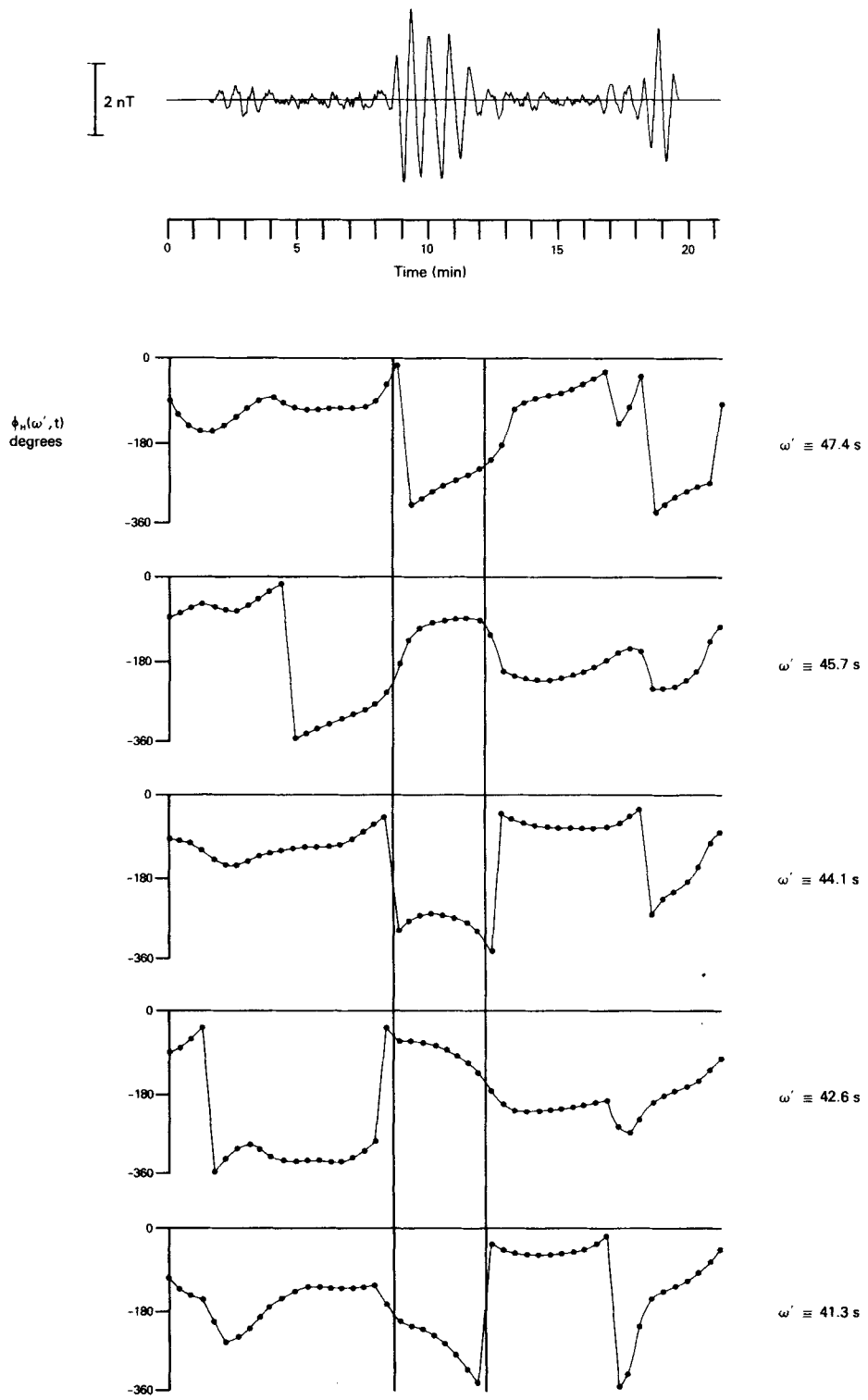

Figure 5. Phase of the demodulated series at five successive central frequencies as a function of time.

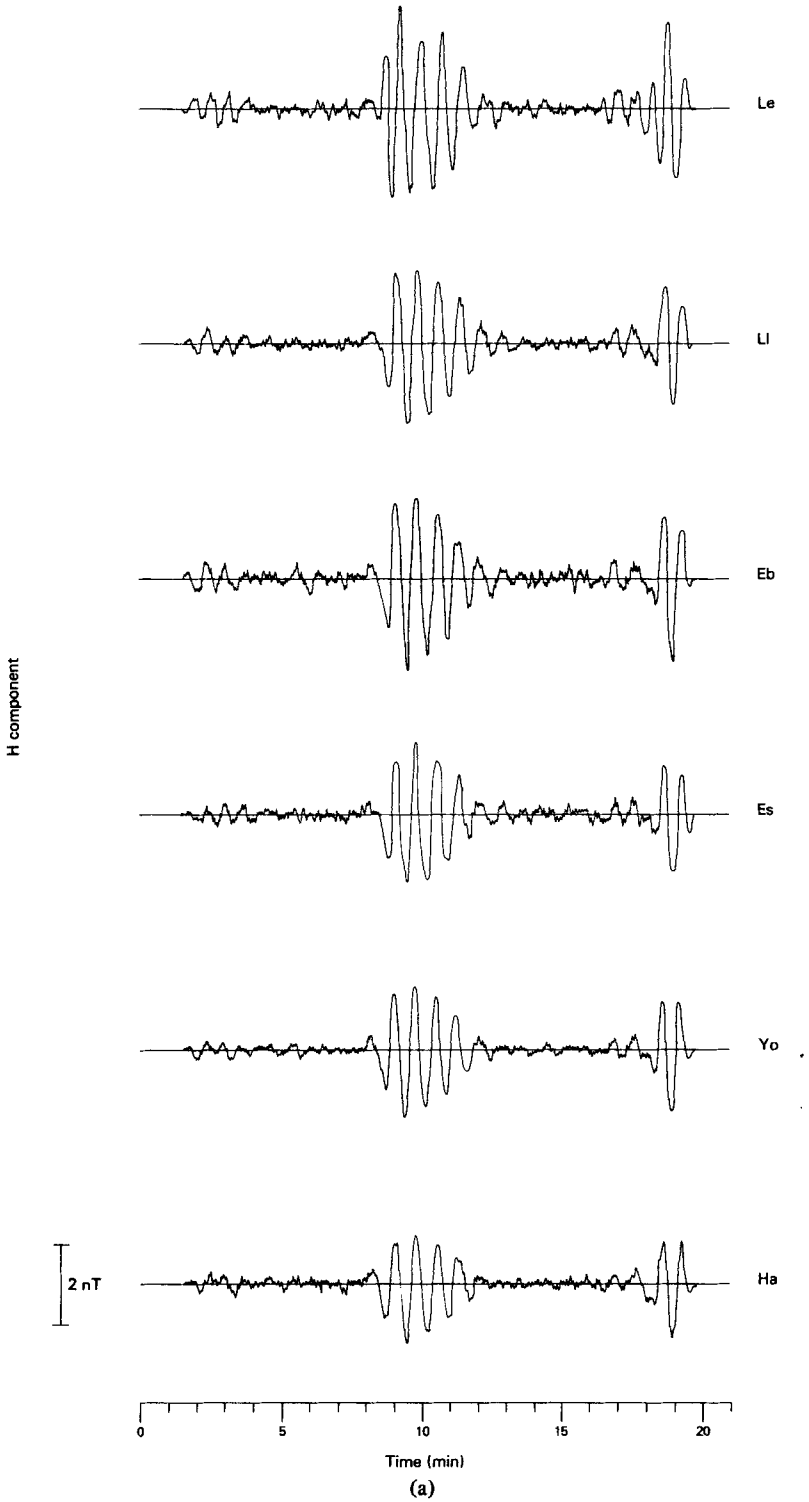

Figure 7. (a) *H*-components of the Pi2 recorded at six stations forming an approximately meridional profile. (b) *D*-component waveforms. Time 0 as for Fig. 3(a).

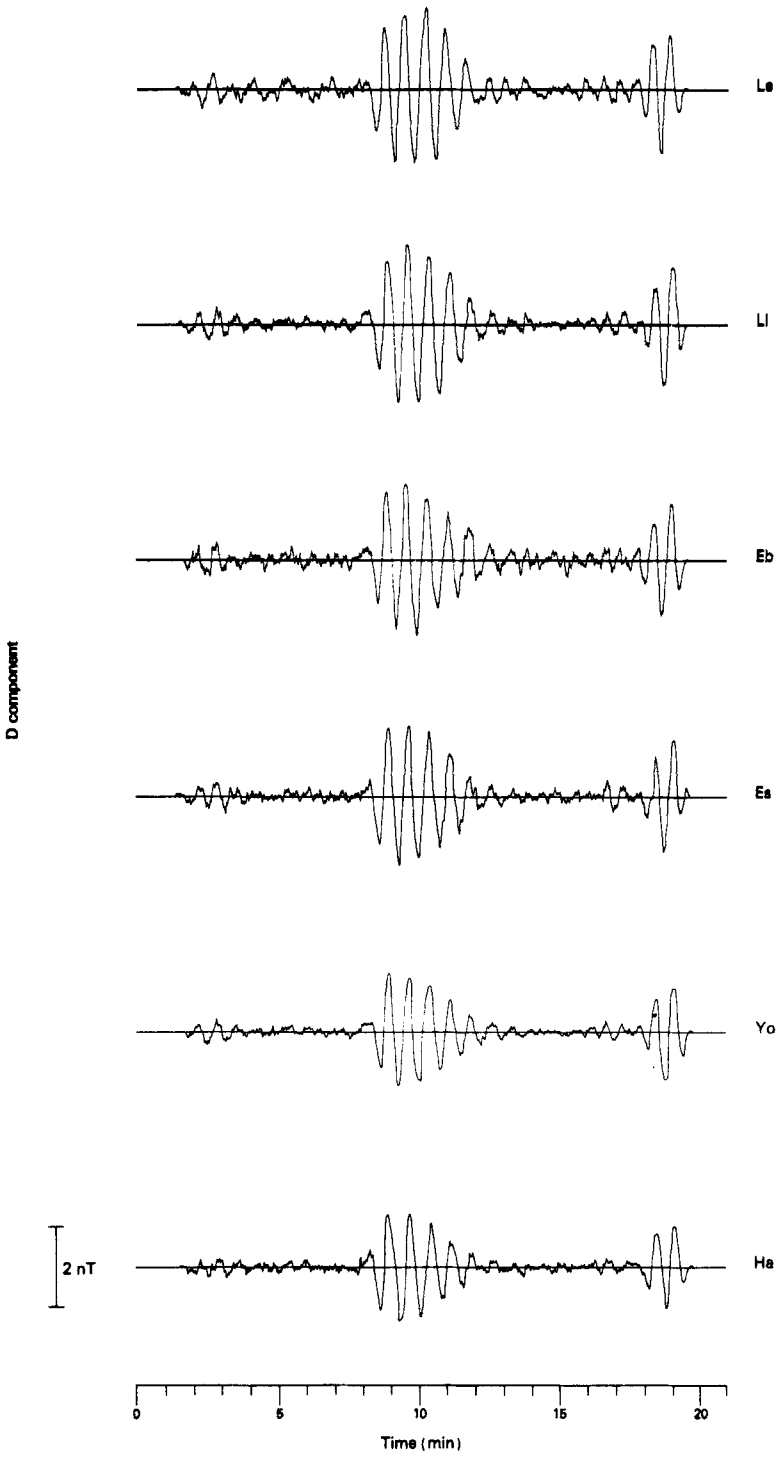

(b)

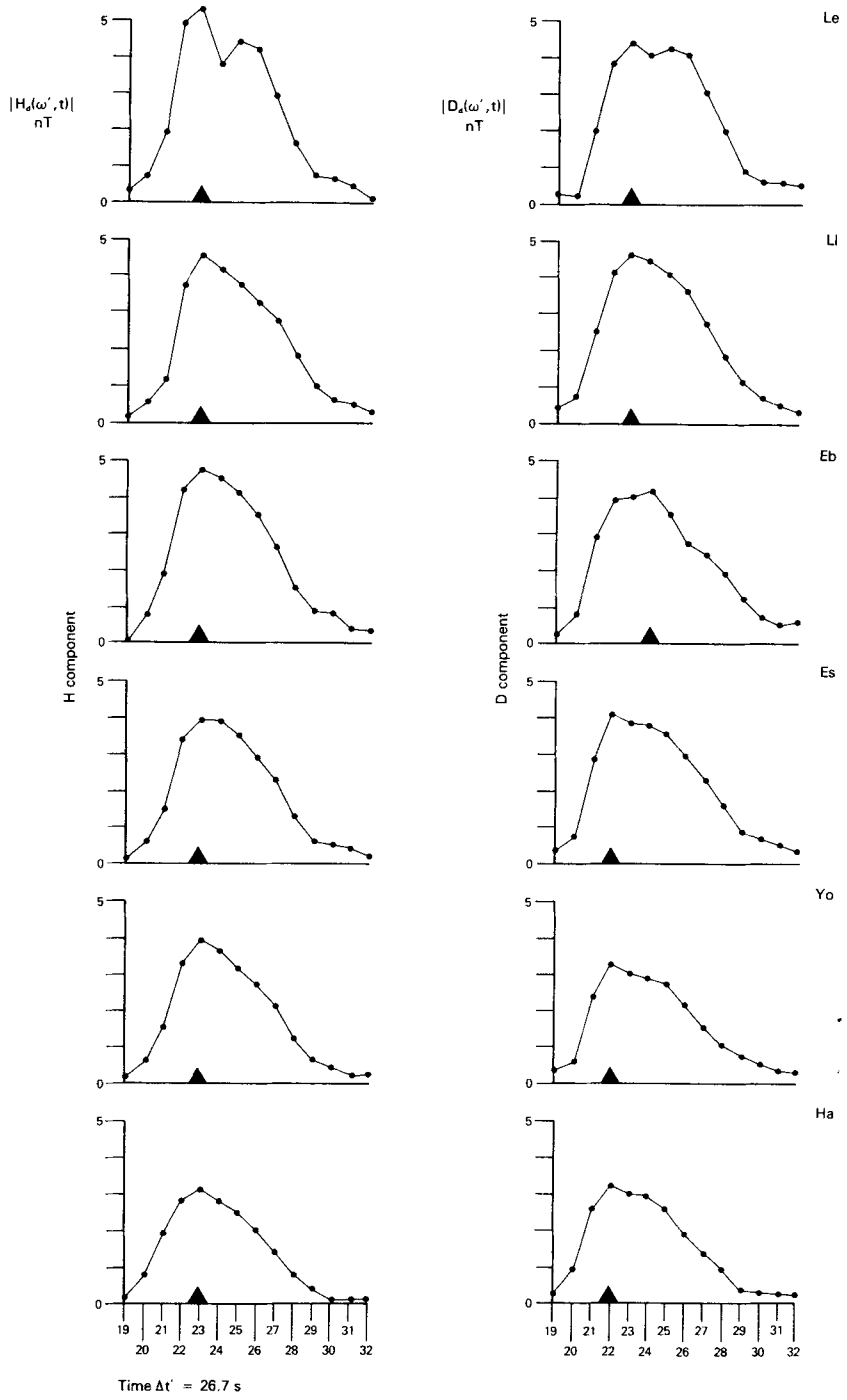

Figure 8. Demodulate amplitudes across the central Pi2 waveforms in the *H* and *D* components as a function of time.

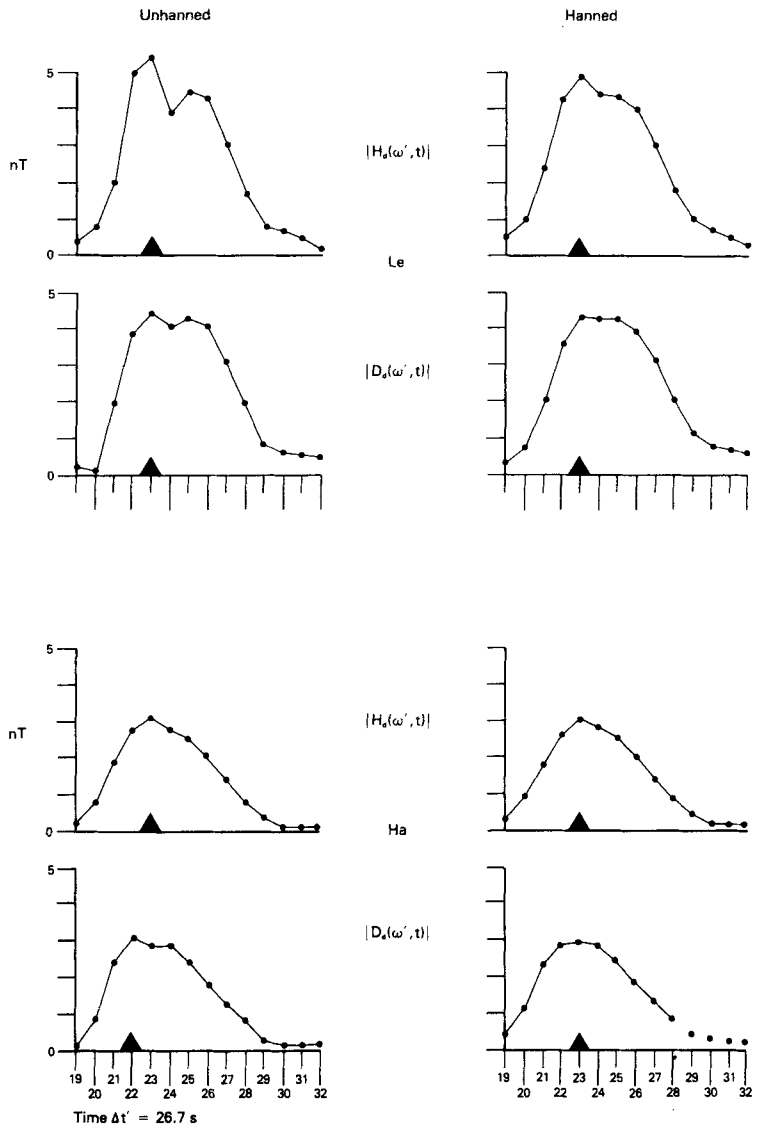

Figure 9. Comparison of Hanned and un-Hanned demodulate amplitudes at the highest and lowest latitude stations, as a function of time.

(c) INTERPRETATION OF PHASE BEHAVIOUR

The phase of the Hanned demodulates ($\phi_d^*(\omega', t)$) for the H and D components is shown in Fig. 10; the time-axis again corresponds to the 14 demodulate estimates across the central waveform. The phase estimates joined by solid lines represent demodulate estimates possessing amplitudes $\geqslant 0.5$ nT. The location of the maximum amplitude is indicated by an arrow. The temporal characteristics of the phase appear consistent at all stations and in both components. The H-component phase demonstrates a clear phase movement between stations *throughout the waveform* while the D-component phase remains similar at all stations. At Le where two amplitude maxima are observed, the H-component phase appears

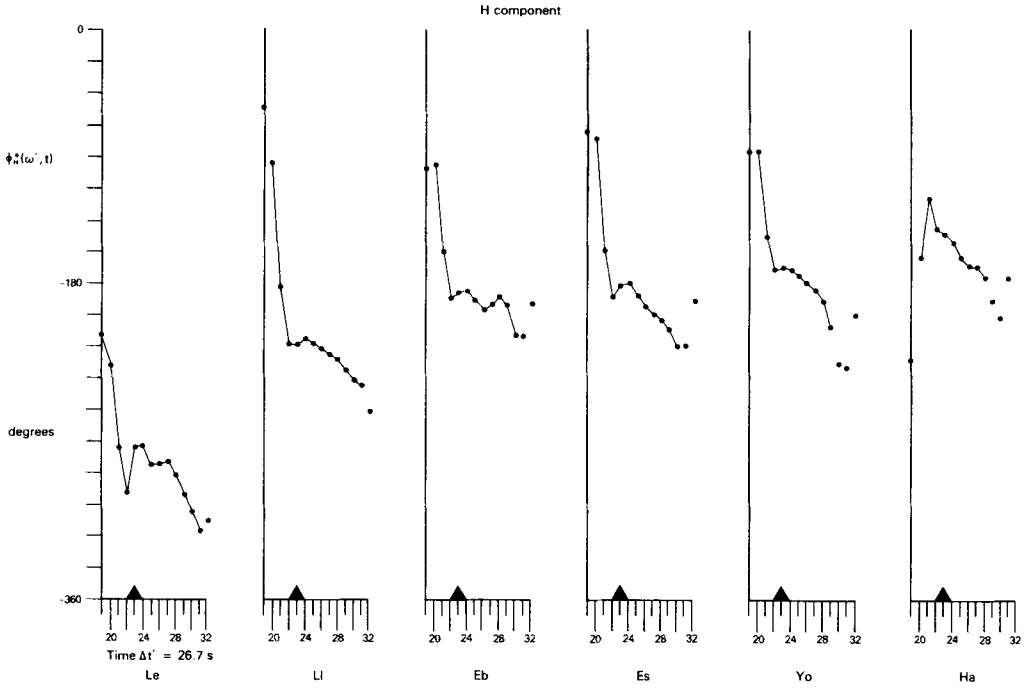

(a)

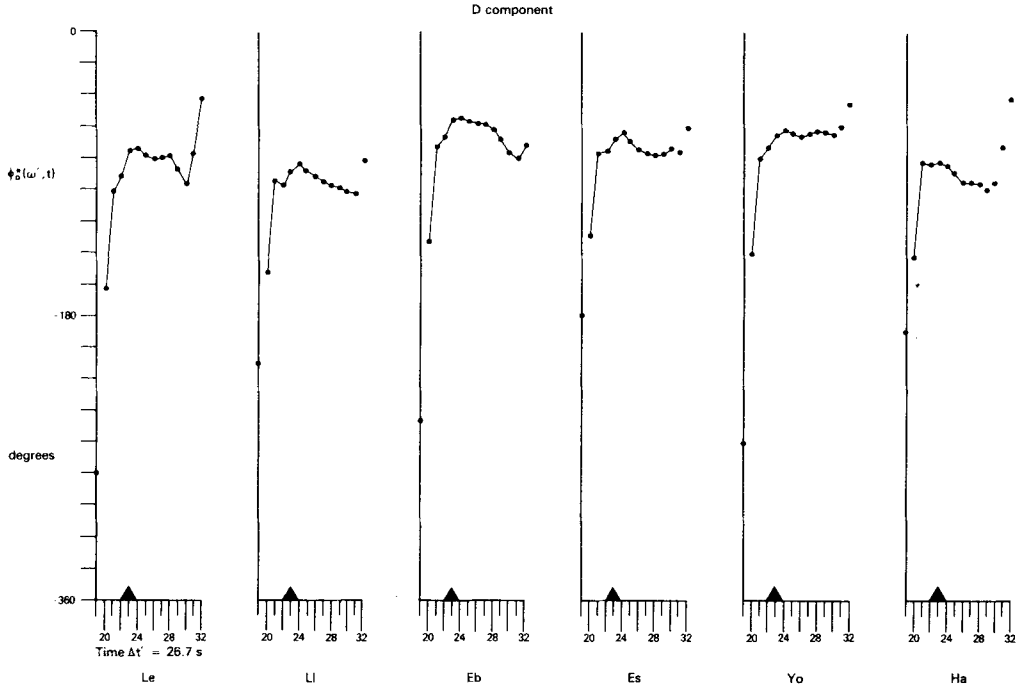

(b)

Figure 10. (a) Phase of the Hanned demodulates in the *H*-component across the central Pi2 waveforms as a function of time. (b) Phase of the Hanned demodulates in the *D*-component.

to go through two of the characteristic 'trends' observed to the south. Hence the amplitude behaviour appears reflected in the phase.

It should be noted that, for the continuous Pi2 waveform here considered, a phase movement with time represents a change of frequency relative to the chosen central frequency. For example, in the *H*-components there is a large phase movement prior to the maximum amplitude. The sense of this phase movement corresponds to a much shorter period than the central period of the analysis which is equivalent to a faster first oscillation of the Pi2. The sense of the phase movement in the *D*-component prior to the maximum amplitude suggests the reverse situation, i.e. a slower first oscillation of the waveform of similar period at all the stations.

(d) COMPARISON WITH CROSS-SPECTRAL PHASE

We next examine the stability of the phase of the demodulate estimates by comparing them with the normally determined cross-spectral phase estimates. The cross-spectral phase estimates are determined between two stations (we here use Le as a reference station) using smoothed spectra such as the one shown in Fig. 3(b). The method is time-global in that the cross-spectral phase estimate at a frequency ω_0 gives the relative phase of all coherent oscillations of frequency ω_0 appearing within the original waveforms. The phase estimates, relative to Le, are plotted against the L value of the six stations in Fig. 11. Three

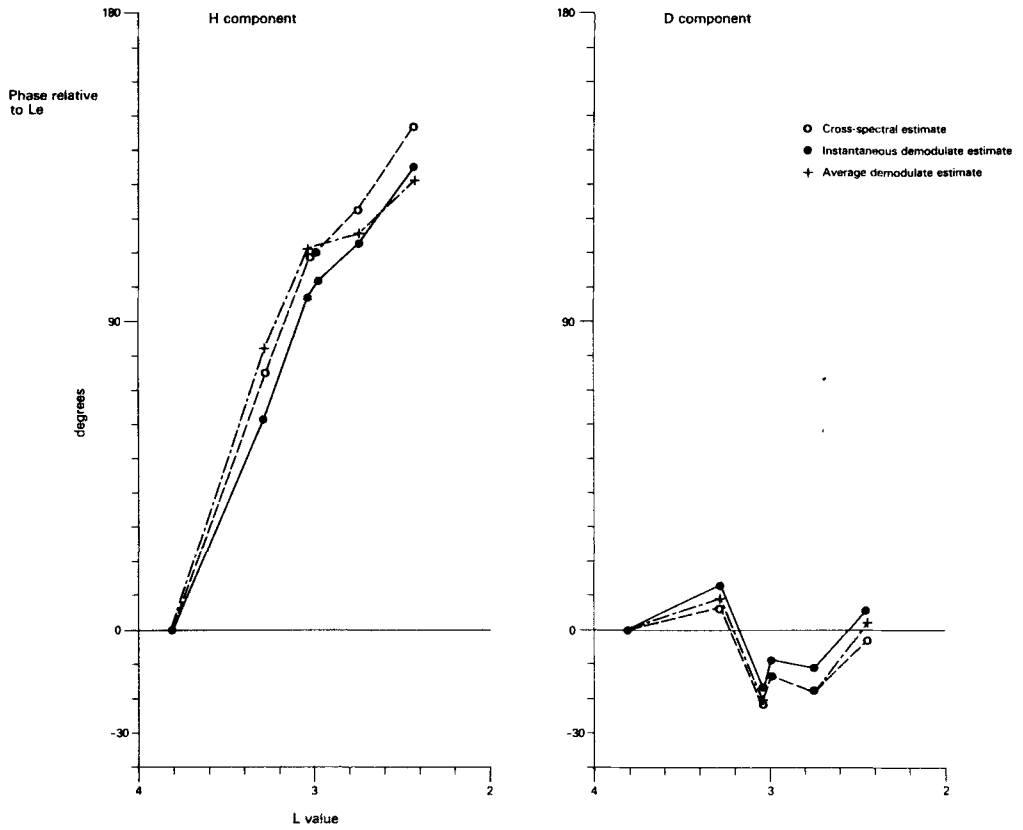

Figure 11. Comparison of cross-spectral and demodulate phase determinations along the meridional profile.

determinations have been made. The first shows the instantaneous phase of the Hanned demodulates at the wave maximum while the second determination is the mean demodulate phase averaged over the five oscillations of the central Pi2 waveform. The third determination shows the cross-spectral phase estimates at the spectral peak, determined using 128 lags. All three determinations are consistent in magnitude and behaviour. Quantitative differences exist of the order of 0 to 15°.

The two averaged determinations are in closer agreement than the instantaneous demodulate phase. The averaged determinations appear, in general, to be positively biased with respect to the instantaneous phase determination at the maximum amplitude. It appears that the instantaneous demodulate estimates are capable of a more detailed and more meaningful resolution than conventional techniques when applied to a dispersive waveform since in this case complex demodulation allows the dispersion (or phase movement) between individual oscillations to be taken into account.

(e) POLARIZATION CHARACTERISTICS

For each instant of time, the complex demodulates in the H and D components can be used to calculate the polarization characteristics of the horizontal field (Banks 1975). We are thus in a position to re-express the amplitude and phase information already presented in terms of the temporal and spatial polarization characteristics of the Pi2 waveforms.

Fig. 12 shows the instantaneous values of the ellipticity at the six stations. The time-axis again corresponds to the 14 Hanned demodulate points across the central waveform. The estimates joined by solid lines represent demodulated points with $|H_d|$ and $|D_d| \geqslant 0.5$ nT. Ellipticities of $+1$ and -1 represent circular waves rotating counter-clockwise and clockwise (looking down along the magnetic field line) respectively. Zero ellipticity corresponds to a wave of linear polarization.

With the exception of the first cycle of the waveform we observe that all cycles rotate clockwise and that the Le waveform is characterized by a linear polarization when compared with the elliptical waveforms at lower latitudes. There is, however, a temporal characteristic that is most in evidence at Le and Es. At the maximum amplitude of the waveform (indicated by the arrow), the ellipticity at Le tends to a minimum value (linear polarization) while at Es, the ellipticity tends to a maximum value (circular rotation). The generation mechanism to be cited predicts a linearly polarized wave at the latitude of the maximum amplitude (i.e. at Le) while away from this 'resonance region' the polarization should tend to a circular nature. This *spatial* behaviour is clearly observed, however, in addition, the dispersive Pi2 waveform exhibits an identical *temporal* characteristic that is most pronounced at Le and Es.

The final piece of polarization information to be presented are the azimuths of the major axis of the horizontal field polarization ellipses which are shown in Fig. 13. Negative and positive azimuths refer to north-west and north-east quadrants respectively. Zero azimuth corresponds to a north–south orientation of the wave. In Fig. 13 we observe that, at the latitude of Es and above, the predominant azimuths are for orientations of $-45°$ in the north-west quadrant. At the lowest latitude station, Ha, the orientation is in the north-east quadrant while at Yo the azimuth is in an intermediate state, changing quadrants midway through the event.

The advantages of using complex demodulation to compute the polarization parameters rather than using the normal time averaged methods (see, e.g. Arthur, McPherron & Means (1976)) are obvious from the figures. The techniques based on cross spectral matrix determinations tend to smear the temporal behaviour of dispersive waveforms over the time

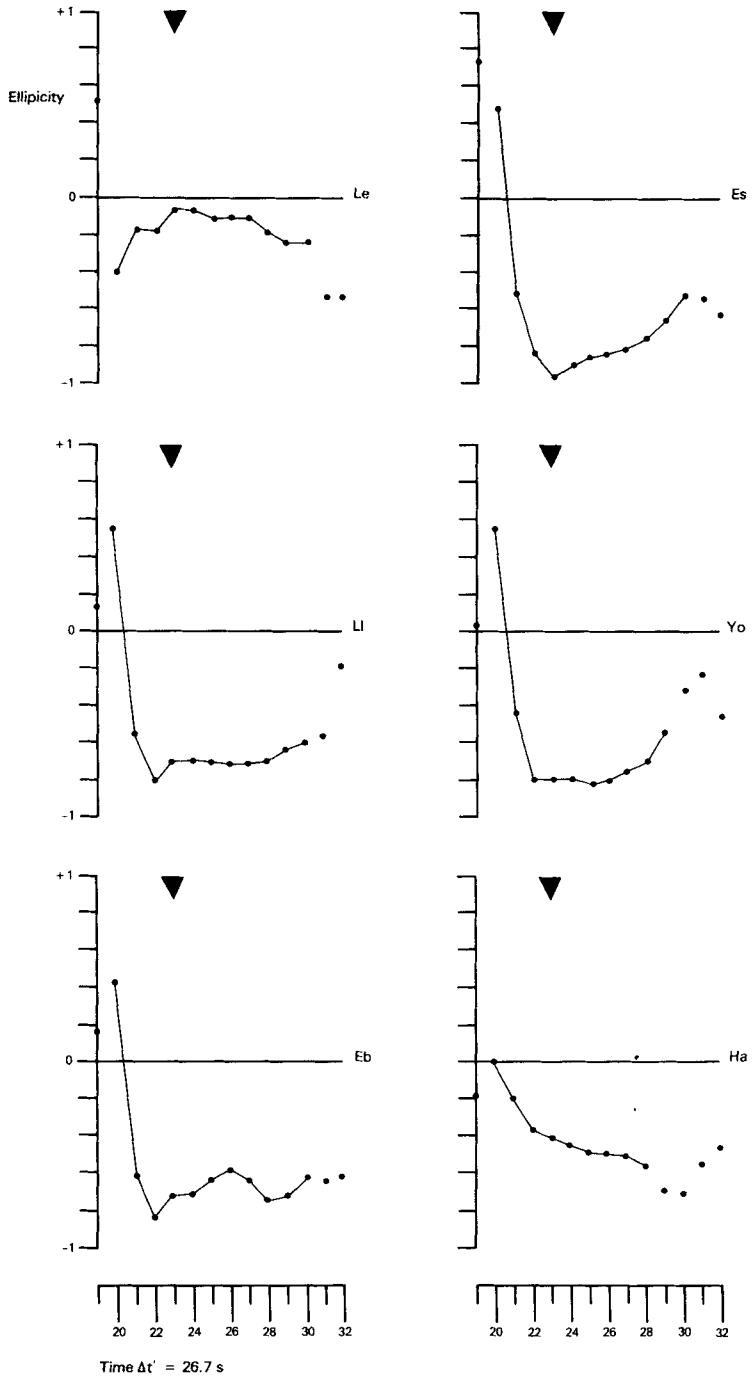

Figure 12. Ellipticity of the Pi2 waveforms at the six stations as a function of time.

interval of the analysis. For a comparison of the polarization characteristics here presented and the more usual hodogram presentation, the reader is referred to figure 10 of Stuart, Brett & Harris (1978) where the wave hodograms of the same Pi2 event are shown.

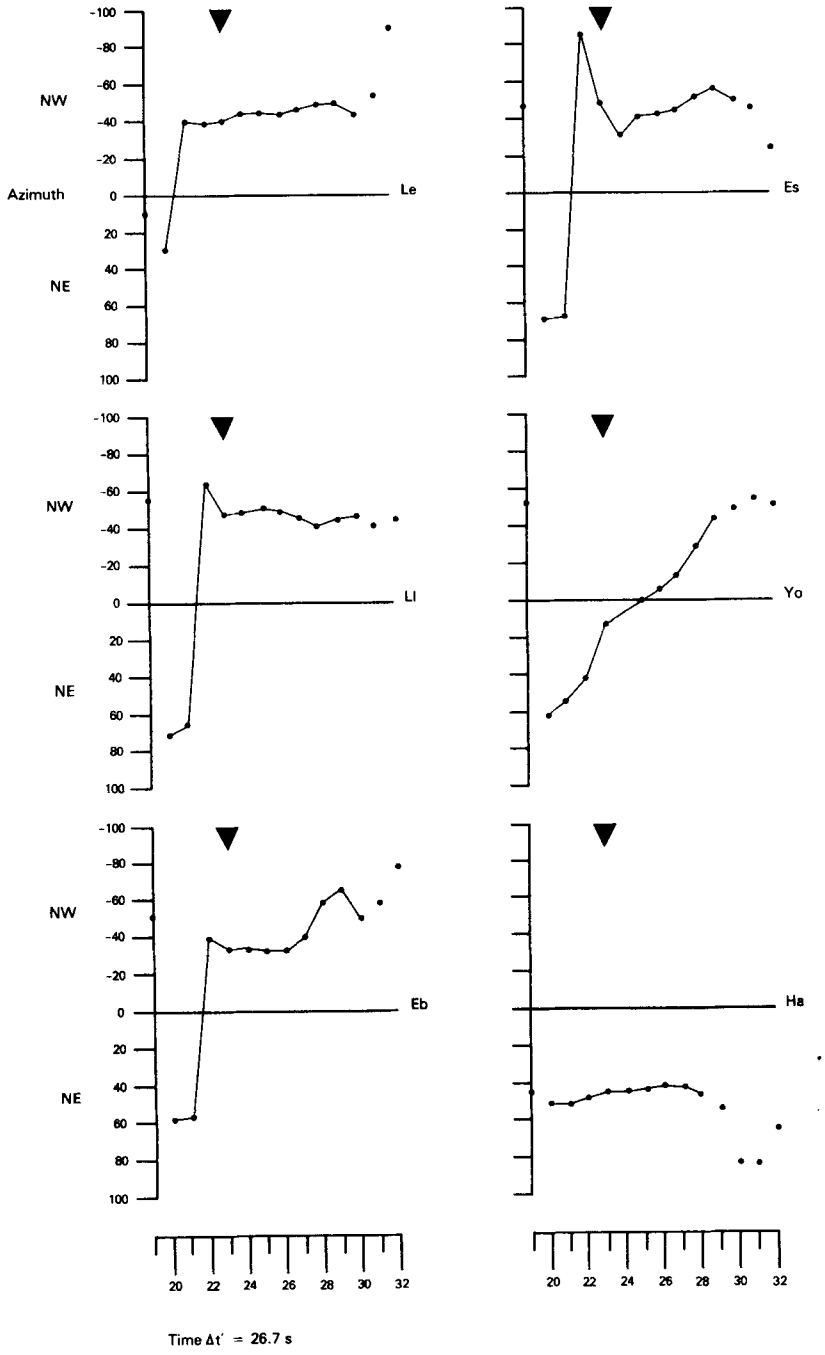

Figure 13. Azimuth of the Pi2 waveforms at the six stations as a function of time.

Discussion

Previous analyses from networks of stations have shown that the maximum amplitude of Pi2 pulsations occurs in the auroral zone (Saito 1969) with a secondary maximum at about

60° latitude (Bjornssen, Hillebrand & Voelker 1971; Fukunishi 1975; Stuart *et al.* 1978). The secondary amplitude maxima occurs within the plasmasphere. The secondary amplitude minimum occurring between auroral and plasmaspheric maxima was found to coincide with a position of wave polarization reversal and has been associated with the plasmapause.

Generally the observational results are consistent with a high latitude generation mechanism similar to that suggested by Rostoker (1967). This mechanism requires the relaxation of a highly distorted magnetic field line. The relaxation produces plasma flow with associated field-aligned currents and a precipitation of particles into the ionosphere. The perturbation in the magnetic field will be seen as in Pi2 and generally the magnetospheric wave modes will be coupled (Orr 1973; Carovillano & McClay 1965). Southwood (1974) and Chen & Hasegawa (1974) have used an approximately monochromatic source at high latitudes to show that it is possible for field lines at mid-latitudes to resonate in the shear Alfvèn wave mode, at a frequency equal to the source frequency, as a result of the change in Alfvèn wave velocity as a function of latitude.

In addition, it has been stressed that ionospheric and atmospheric modification of the waves, particularly in the resonance region, must be taken into account when observing on the ground (Hughes 1974; Hughes & Southwood 1976a, b). These three papers make clear predictions in terms of the amplitude, phase and wave polarization characteristics observed on the ground in the vicinity of a field line resonance. If we accept that we are observing a plasmaspheric resonance in the region of the plasmapause we can relate our observations to the ionospheric modifications predicted by Hughes & Southwood (1976b).

Hughes & Southwood examine the relative importance of ionospheric effects on the relation between a source signal in the magnetosphere and a pulsation observed on the ground. The model used is the transverse field line resonance mode of Southwood (1974). Within the magnetosphere, this resonance occurs in the *D*-component. The main ionospheric effect is to produce a left-hand 90° rotation between magnetosphere and ground such that amplitude and phase motion are observed in the *H*-component in the vicinity of a resonance. Although both *H* and *D* components show an amplitude decay away from the resonance maximum (Le) (Fig. 8), the phase motion is confined almost entirely to the *H*-component (Fig. 10).

The lateral scale on which the resonance structure occurs is $\epsilon \sim (\gamma/\omega)l$, where γ is the damping decrement of the transverse Alfvèn wave (angular frequency ω) in the absence of a source and l is the scale of variation of the Alfvèn velocity across the field lines (Hughes & Southwood 1976b). The width of the resonance region may be defined since a total phase motion of 180° should occur on the scale $2|\epsilon|$ (Southwood 1975). In the present study we have observations only to the south of resonance. However, examination of Fig. 11 shows that a phase change of 90° occurs between Le and Eb giving a maximum value of $\epsilon \sim 440$ km.

In obtaining the temporal characteristics of the ellipticity (Fig. 12) we have a second determination on the width of the resonance region if ϵ is defined as the distance between stations recording ellipticities of 0 and ± 1. In this case a maximum determination of ϵ is given by the distance between Le and Es which is comparable with the above determination.

In the absence of ionospheric modification of a magnetospheric resonance, a reversal in the sense of rotation (change in sign of ellipticity) is predicted as one moves through the resonance region. No such spatial reversal is observed although a temporal one is evident within the resonance region (Fig. 12). The lack of spatial reversal can be explained by too great a station spacing or by a type of ionospheric modification as predicted by Hughes & Southwood.

The final result compared is the azimuthal variation with latitude shown in Fig. 13. The

models used by Hughes & Southwood predict a north-west quadrant for the azimuth *within* the resonance region (for local morning westward travelling wave events) if the local Alfvèn resonance frequency increases with increasing latitude as it does at the plasmapause. This is observed as far south as Es which again experimentally verifies the width of the resonance region. For strong energy dissipation (γ and ϵ large) Hughes & Southwood note that south of the resonance region the azimuth changes quadrant as is observed between Es and the lowest latitude station Ha and indicates significant energy flow away from the resonance.

Further work investigating the non-stationary behaviour of continuous day-time pulsations over a larger array of stations is under way.

Conclusions

The application of complex demodulation techniques to dispersive waveforms has been discussed and some detailed temporal characteristics of a particular Pi2 micropulsation investigated. Frequency dispersion can be adequately quantified by the method provided sufficient care is taken over band-pass filter design. The resulting amplitude and phase information can be interpreted more meaningfully than cross-spectral information which is necessarily time-averaged. The method also lends itself to the derivation of polarization characteristics. In addition to the spatial variation of polarization characteristics through a resonance region afforded by a magnetometer array, identical temporal effects at particular sites have been observed. The results obtained are consistent with the current theories on the ionospheric modification of a given magnetospheric source resonance.

The agreement with the theory together with the large spatial width of the resonance region (~ 440 km) observed on the ground, suggests that the night-time ionosphere is capable of a distinct modification of a magnetospheric wave. We therefore suggest that the resolution afforded by complex demodulation can be of direct value if ground observations of pulsations are to be used for the determination of magnetospheric plasma conditions.

Another advantage of complex demodulation is that it offers a method for obtaining a selection criterion in terms of a signal/noise ratio. The general background level of the modulus of the complex demodulates can be observed and only those demodulates significantly above this noise level can be selected and used to compute the wave polarization characteristics. Such an investigation has been carried out and will be reported in a companion paper.

Acknowledgments

The authors would like to thank Drs W. F. Stuart and D. Orr for many helpful discussions and suggestions and the SRC for grant support under contract SGD00178. This type of work is only made possible by the help and diligence of observatory personnel to whom we express our gratitude.

References

Arthur, C. W., McPherron, R. L. & Means, J. D., 1976. A comparative study of three techniques for using the spectral matrix in wave analysis, *Rad. Sci.*, **11**, 833–845.

Banks, R. J., 1975. Complex demodulation of geomagnetic data and the estimation of transfer functions, *Geophys. J. R. astr. Soc.*, **43**, 83–101.

Bingham, C., Godfrey, M. D. & Tukey, J. W., 1967. Modern techniques of power spectrum estimation, *IEEE Trans. Audio Electr.*, **AU-15**, 56.

Bjornssen, A., Hillebrand, O. & Voelker, H., 1971. First observational results of geomagnetic Pi2 and Pc5 pulsations on a north–south profile through Europe, *Z. Geophys.*, **37**, 1031–1042.

Carovillano, R. L. & McClay, J. F., 1965. Hydromagnetic eigenmodes in multipole fields, *Phys. Fluids*, **8**, 2006–2013.

Chen, L. & Hasegawa, A., 1974. A theory of long period magnetic pulsations, 1. Steady state excitation of field line resonance, *J. geophys. Res.*, **79**, 1024–1032.

Cooley, J. W., Lewis, P. A. W. & Welch, P. D., 1967. The fast Fourier transform algorithm and its applications, *Research paper RC-1743*, IBM Watson Research Center, Yorktown Heights, New York.

Fukunishi, H., 1975. Polarisation changes of geomagnetic Pi2 pulsations associated with the plasmapause, *J. geophys. Res.*, **80**, 98–110.

Hughes, W. J., 1974. The effect of the atmosphere and ionosphere on long period magnetospheric micropulsations, *Planet. Space Sci.*, **22**, 1157–1172.

Hughes, W. J. & Southwood, D. J., 1976a. The screening of micropulsation signals by the atmosphere and ionosphere, *J. geophys. Res.*, **81**, 3234–3240.

Hughes, W. J. & Southwood, D. J., 1976b. An illustration of modification of geomagnetic pulsation structure by the ionosphere, *J. geophys. Res.*, **81**, 3241–3247.

Orr, D., 1973. Magnetic pulsations within the magnetosphere: a review, *J. atmos. terr. Phys.*, **34**, 1–50.

Rostoker, G., 1967. The frequency spectrum of Pi2 micropulsation activity and its relationship to planetary magnetic activity, *J. geophys. Res.*, **72**, 2032–2039.

Saito, T., 1969. Geomagnetic pulsations, *Space Sci. Rev.*, **10**, 319–412.

Southwood, D. J., 1974. Some features of field line resonances in the magnetosphere, *Planet. Space Sci.*, **22**, 483–491.

Southwood, D. J., 1975. Comments on field line resonances and micropulsations, *Geophys. J. R. astr. Soc.*, **41**, 425–431.

Stuart, W. F., Brett, P. M. & Harris, T. J., 1978. Mid-latitude secondary resonance in Pi2's, *J. atmos. terr. Phys.*, in press.

Stuart, W. F., Sherwood, V. & Mackintosh, S. M., 1971. The power spectral density technique applied to micropulsation analysis, *Pure Appl. Geophys.*, **92**, 150–164.

Tukey, J. W., 1961. Discussion, emphasizing the connection between analysis of variance and spectrum analysis, *Technometrics*, **3**, 191–219.